Synthetic and Systems Biotechnology 10 (2025) 583–592

Contents lists available at ScienceDirect

Synthetic and Systems Biotechnology

journal homepage: www.keaipublishing.com/en/journals/synthetic-and-systems-biotechnology

Original Research Article

CRISPRi-mediated multigene downregulating redirects the metabolic flux to spinosad biosynthesis in *Saccharopolyspora spinosa*

Zirong Zhu [a,1], Li Cao [a,1], Ziyuan Xia [a], Xirong Liu [b], Wangqion Chen [a], Zirui Dai [a], Duo Jin [a], Jie Rang [a], Shengbiao Hu [a,*], Liqiu Xia [a,**]

[a] College of Life Science, Hunan Normal University, Hunan Provincial Key Laboratory of Microbial Molecular Biology, Changsha, 410081, Hunan, China
[b] Hunan Norchem Pharmaceutical Co., Ltd, Changsha, Hunan, 410205, China

ARTICLE INFO

Keywords:
Saccharopolyspora spinosa
Spinosad biosynthesis
Simultaneous multigene knockdown
Pyruvate carboxylase
Metabolism regulation

ABSTRACT

Microorganisms are often likened to complex production workshops. In *Saccharopolyspora spinosa* (*S. spinosa*), the biosynthesis of spinosad is a production line within its intricate workshop. Optimizing the entire production environment and reducing unnecessary metabolic flow is essential to increasing spinosad yield. Pyruvate serves as a crucial precursor for spinosad biosynthesis. Previous studies revealed that the *pyc* gene is highly expressed in the gluconeogenic pathway, leading to a pyruvate shunt. By downregulating *pyc*, we enhanced spinosad yield, although the improvement was below expectations. We speculated that most of the accumulated pyruvate following the *pyc* knockdown entered some synthetic pathways unrelated to spinosad. Through metabolic pathway and qRT-PCR analyses, we found that the expression levels of *gltA1* and *atoB3* within the pyruvate metabolic tributary, including the TCA cycle and ethylmalonyl-CoA pathway, were significantly increased in the *pyc* knockdown strain. The combined knockdown of these three genes optimized the spinosad production line, increasing its yield to 633.1 ± 38.6 mg/L, representing a 199.4 % increase. This study identifies three key genes for optimizing spinosad biosynthesis and offers insights into gene screening and the efficient construction of Spinosad-producing strains.

1. Introduction

To maintain normal growth and development, strains have generated efficient methods to balance the expression of various genes during evolution [1]. This balance is achieved by fine-tuning the expression levels of enzyme-coding genes, as their expression levels typically influence the efficiency of many essential metabolic pathways [2]. However, to optimize the production of desired compounds in bacteria, various synthetic systems are often constructed or enhanced, which can disrupt the balance of gene expression. This disruption may damage the fine-tuned regulatory networks and produce toxic intermediates, thereby inhibiting bacterial growth and development [3]. Responsible for the production of approximately 70 % of the world's natural products [4,5], actinomycetes' metabolic networks have garnered significant attention. Properly regulating the expression levels of key genes in various natural product metabolic pathways is therefore of great significance. In particular, balancing cellular metabolism through metabolic engineering is essential for increasing the productivity of target products.

To optimize the efficiency of value-added product production, synthetic biological methods and metabolic engineering strategies are widely used to regulate cell metabolism and develop highly efficient microbial cell factories [6,7]. For examples, Stegmüller et al. applied several rounds of metabolic engineering in *Streptomyces albidoflavus* to streamlined the key genes involved in the pentose phosphate pathway, the shikimic acid pathway, CoA esters supply, nybomycin biosynthesis, and export, while removing four *nyb* regulatory genes, leading to a 15-fold increase in nybomycin [8]. Similarly, Wang et al. designed a metabolic engineering strategy based on metabolomics and transcriptomics in *Streptomyces albulus*, which enhanced the expression of ε-Poly-L-lysine (ε-PL) synthetase and improved ATP and l-lysin supply, thereby significantly boosting the production of ε-PL [9]. Furthermore,

Peer review under the responsibility of Editorial Board of Synthetic and Systems Biotechnology.
* Corresponding author.
** Corresponding author.
E-mail addresses: shengbiaohu@hunnu.edu.cn (S. Hu), xialq@hunnu.edu.cn (L. Xia).
[1] These authors contributed equally to this study.

https://doi.org/10.1016/j.synbio.2025.02.010
Received 7 October 2024; Received in revised form 24 January 2025; Accepted 17 February 2025
Available online 20 February 2025

Zhuang et al. achieved a titer of 43.5 ± 2.4 mg/L for anthraquinone-fused enediynes in *Streptomyces* sp. CB03234–S by inactivating seven potential precursor competitive biosynthetic gene clusters and overexpressing five essential biosynthetic genes [10].

The key to the success of synthetic biology and metabolic engineering lies in achieving an optimal distribution of metabolic flux within the microbial metabolic network [11]. Over the past two decades, traditional strategies such as knocking out key genes in precursor competition pathways and enhancing the expression levels or increasing the copy numbers of key genes in target metabolic pathways have been widely employed to maximize the titer of target products [12,13]. However, for natural products involving more complex metabolic pathways, these traditional approaches often lead to metabolic imbalances, resulting in slow cell growth, an excessive metabolic burden from intermediates, or the production of toxic intermediates or byproducts, thus limiting the yield of target metabolites [14–16]. In such cases, redirecting metabolic flux through the down-regulation of essential precursor competitive metabolic pathways can effectively balance the flux between cell growth and target product biosynthesis [17,18], thereby alleviating intracellular metabolic pressure and optimizing the utilization of metabolic flux.

Spinosad is a macrolide secondary metabolite produced through the aerobic fermentation of *Saccharopolyspora spinosa* (*S. spinosa*), characterized by high insecticidal activity, and it has been widely applied in food storage and crop pest control [19–22]. The biosynthesis gene cluster of Spinosad, along with its biosynthesis pathway, has been described in detail [23]. The biosynthetic process of spinosad competes for common precursors with essential pathways, particularly those involved in central carbon metabolism [24]. However, primary metabolism often takes precedence over secondary metabolism in metabolic flux allocation [25] and these precursors are critical for cell growth, making it unfeasible to directly knock out genes in essential primary metabolic pathways. To address this, the CRISPR interference (CRISPRi) system, which employs the CRISPR/Cas system with a deactivated endonuclease Cas9 (dCas9) [26,27], was used in this study. This approach coordinated the balance between primary and secondary metabolism by down-regulating, rather than deleting, genes in precursor competing pathways, thereby redirecting metabolic flux toward spinosad biosynthesis and preventing the excessive accumulation of intermediates or toxic by-products.

According to the previous transcriptomic analysis of *S. spinosa* CCTCC M206084 (GenBank accession no. CP061007) [28], key rate-limiting enzymes in gluconeogenesis (a pathway competing with pyruvate), the EMC pathway and the TCA pathway (downstream acetyl-CoA competing pathways), exhibited high transcription levels during the three selected phases. Therefore, CRISPRi-mediated regulation was applied to downregulate the key nodes in these three metabolic pathways to promote spinosad biosynthesis. The spinosad titer was further improved by screening sgRNA combination libraries with different inhibitory strengths, and the underlying mechanisms promoting spinosad biosynthesis were elucidated using proteomic analysis. This study demonstrated the feasibility of balancing multiple critical pathways in *S. spinosa* using the CRISPRi system, offering a novel approach for the metabolic engineering of spinosad-like biosynthetic processes.

2. Materials and methods

2.1. Strains, plasmids, primers, medium and culture conditions

The wild-type strain *S. spinosa* used in this study was stored in our lab. All the strains used in this research are listed in Table S1. The plasmids and primers used in this study are listed in Table S2 and Table S3, respectively. All *Escherichia coli* (*E. coli*) strains were cultured in lysogeny broth (LB) at 37 °C. CSM medium [29] and SFM [30] were used for seed culture and fermentation of *S. spinosa* and its derived strains, respectively. All *S. spinosa* strains were cultured at 30 °C, 260 rpm. All media used to culture the strains containing the pSET-*ermE**p-*dcas9*-fd (abbreviated as pSET-*dcas9*) vector [31] need to add apramycin (50 μg/mL). TSB medium (tryptic soy broth medium) and R6 medium [32] were used for intergeneric conjugative transfer between *E. coli* S17-1 and *S. spinosa*.

2.2. Detection of biomass, precursors, and spinosad

The detection of biomass, pyruvate, short-chain acyl-CoA, and spinosad was conducted according to methods described in our previous studies [28,30,32,33]. The titers of spinosad, pyruvate, and short-chain acyl-CoA were calculated using their respective standard curves. The standard spinosad was purchased from MERCK. (Fig. S1).

2.3. Construction of recombinant plasmids and engineering strains

All gene downregulation CRISPRi plasmids were constructed by replacing the 20-nt specific guide sequence of sgRNA in the non-template strand of the target genes, as described on the CRISPR direct web (http://crispr.dbcls.jp/) [34]. For example, the construction process of pSET-*dcas9-sg-pyc* is as follows. Primer pairs F-*sg-pyc*/R-sgRNA and the plasmid pSET-*dcas9* were used to amplify the sgRNA containing the 20-nt specific guide sequence targeting *pyc* through PCR (Fig. S2). The pSET-*dcas9* plasmid [31] and amplified sgRNA were digested using restriction enzymes *Spe*I and *Eco*RI. Following purification, the target sgRNA was ligated into the corresponding restriction sites of pSET-*dcas9* using T4 DNA ligase, resulting in the vector pSET-*dcas9-sg-pyc*. The recombinant plasmid pSET-*dcas9-sg-pyc* was introduced into *E. coli* S17-1 and subsequently transferred into *S. spinosa* via intergeneric conjugative transfer. The construction of other single-gene downregulation CRISPRi plasmids involved modifying only the 20-nt specific guide sequences based on the target genes and using upstream primers to amplify sgRNA. Combination inhibition fragments were assembled and integrated into pSET-*dcas9* by GenScript Biotechnology Co., Ltd., Nanjing, China. Complete sequences and related descriptions are provided in the Supplementary Materials.

The specific procedures for conjugation transfer are as follows: (1) 1 mL of *S. spinosa* was activated for 48 h in 20 mL of CSM medium and subsequently transferred to TSB medium for 12 h at a 10 % inoculum volume. Meanwhile, *E. coli* S17-1 containing the recombinant plasmid was activated for 12 h in LB medium. (2) After 12 h of culture, *S. spinosa* was inoculated into 20 mL of TSB medium at a 20 % inoculum volume, and *E. coli* S17-1 was inoculated into LB medium at a 2 % inoculum volume. Both strains were cultured for 4 h (3) All the activated *S. spinosa* cells were transferred into a sterilized 50 mL centrifuge tube, centrifuged at 8000 rpm for 15 min, and the supernatant was discarded. Then, 25 mL of fresh TSB medium was added for washing and resuspension of the *S. spinosa*. The cells were centrifuged again at 8000 rpm for 15 min, the supernatant was discarded, and the *S. spinosa* cells were collected. The same procedure was followed for *E. coli* S17-1, and the step was repeated 2–3 times. (4) Twenty milliliters of TSB solution was added to resuspend *S. spinosa* and *E. coli* S17-1, respectively. *E. coli* S17-1 cells were diluted 20 × , 40 × , 80 × , 160 × , and 250 × , respectively, and then mixed with *S. spinosa* at a 1:1 ratio (total volume of 1 mL). The mixture was centrifuged at 8000 rpm for 15 min, leaving approximately 100 μL of suspension. (5) The 100 μL suspension was spread onto R6 agar medium plates and cultured for 14 h. Then, 1 mL of sterile water containing 0.1 mg of nalidixic acid and 0.05 mg of apramycin was evenly spread onto each plate. The plates were then incubated for 7–12 days until transformants appeared.

2.4. Total RNA extraction and RT-qPCR analysis

Total RNA from *S. spinosa* and its derived strains was extracted on the 2nd, 4th, 6th, and 8th days using the Total RNA Extractor kit (Sangon). The purity and concentration of the extracted RNA were measured using

a NanoDrop 2000 spectrophotometer (Thermo). The total RNA was reverse-transcribed into cDNA using the Reverse Transcription Premix Kit (Accurate Biology Co., Ltd., Changsha, China). The 7500 Real-Time PCR System (Applied Biosystems, USA) was used to monitor the fluorescence intensity of the samples in real-time. The 16S rRNA gene was used as the endogenous control. Each experiment was performed in triplicate.

2.5. Protein detection and LC– MS/MS bioinformatic analysis

The *S. spinosa*-pSET-*dcas9/sg-pyc/sg-gltA11/sg-atoB3* and *S. spinosa* CCTCC M206084 were harvested (8000× *g*, 10 min, 4 °C) after 144 h of culture, washed four times with phosphate-buffer saline (PBS), and quickly frozen in liquid nitrogen. The extraction, quality verification, and digestion of proteins were performed in Wininnovate Biotechnology Co., Ltd., Shenzhen, China. The specific procedure followed the description in our previous study [30].

3. Results

3.1. CRISPRi-mediated inhibitory circuit downregulates the gluconeogenesis

To minimize precursor competition in spinosad biosynthesis, the CRISPRi system was utilized to construct a multigene simultaneous downregulation circuit (Fig. 1A). Key nodes in three fundamental pathways—gluconeogenesis, the TCA cycle, and the EMC pathway—were downregulated using the CRISPRi multigene repression circuit. This intervention shifted carbon flux from primary metabolism to spinosad biosynthesis, thereby enhancing spinosad production (Fig. 1B). Before targeting specific genes, the potential cytotoxicity of the CRISPRi system was evaluated. The introduction of an empty vector into *S. spinosa* resulted in no significant changes in biomass or spinosad titer (Fig. S3), demonstrating that the CRISPRi system does not adversely affect cell viability or spinosad biosynthesis.

As the final product of glycolysis, pyruvate plays a critical role in spinosad biosynthesis [28,35,36]. However, under the catalysis of pyruvate carboxylase (EC 6.4.1.1), pyruvate can be converted into oxaloacetate via the gluconeogenesis pathway for intracellular metabolic

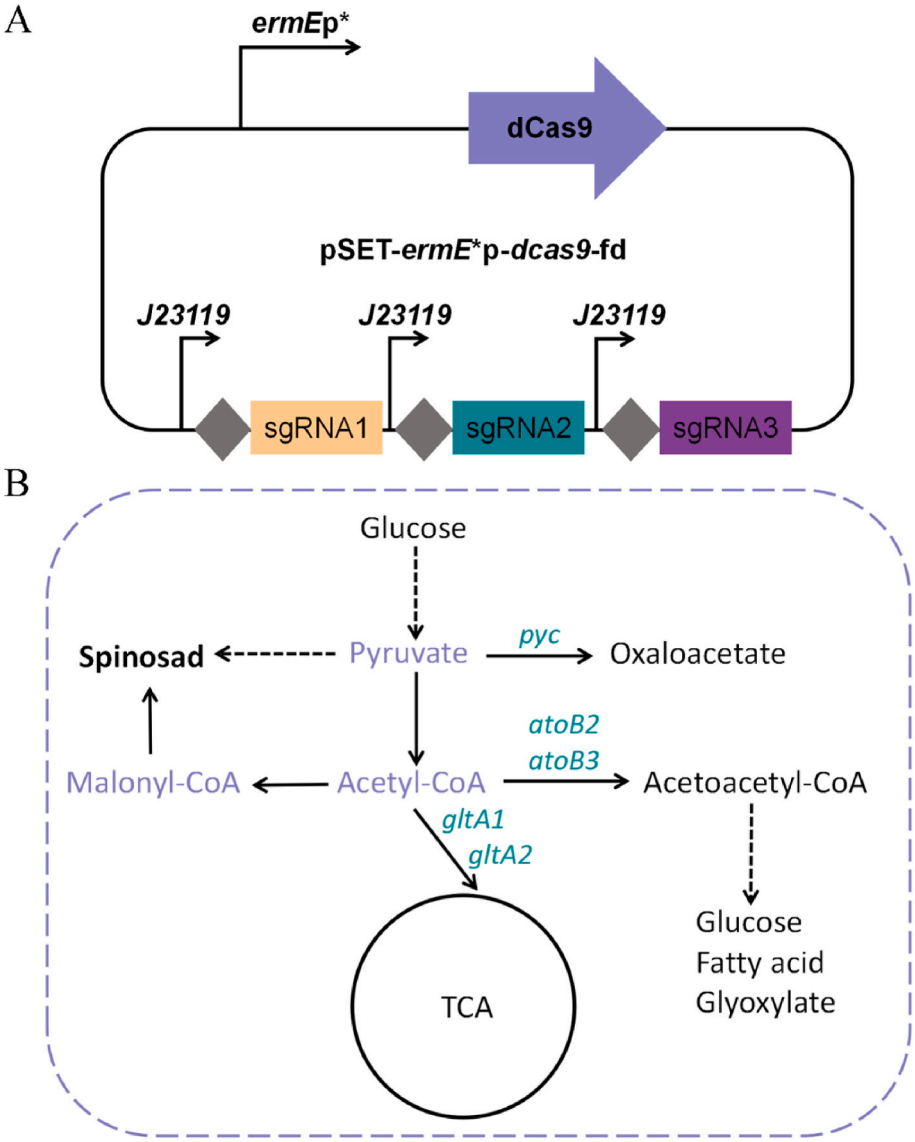

Fig. 1. Schematic design of multigene downregulation CRISPRi cuicut. **(A)** Multigene downregulation CRISPRi cuicut. **(B)** Schematic diagram of some essential metabolic pathways in *S. spinosa*.

replenishment. Our previous transcriptomic analysis revealed that the *pyc* gene (encoding pyruvate carboxylase) exhibited high transcription levels during three stages of *S. spinosa* growth: T1 (logarithmic growth phase, 48 h), T2 (early stationary phase, 96 h), and T3 (late stationary phase, 192 h) (Fig. S4). Moreover, the genome of *S. spinosa* CCTCC M206084 contains only one *pyc* gene (orf 03273-1979). Consequently, *pyc* was downregulated using CRISPRi to enhance pyruvate flux redirection towards spinosad biosynthesis.

The sgRNA for *pyc* (*sg-pyc*) was designed targeting nt 793–812 downstream of the start codon, and the recombinant plasmid (pSET-*dcas9/sg-pyc*) was introduced into *S. spinosa* CCTCC M206084. The spinosad production in *S. spinosa*-pSET-*dcas9/sg-pyc* (the *pyc* downregulated strain) reached 418.8 ± 26.7 mg/L, representing a 31.9 % increase compared to the control strain, with no significant change in biomass (Fig. 2A and B). Meanwhile, RT-qPCR results indicated that the relative expression levels of the *pyc* gene in all four selected growth phases were reduced to 21.8 %–31.1 % of their original levels (Fig. 2C). These findings provided initial evidence that downregulation of the pyruvate competition pathway in *S. spinosa* can enhance spinosad biosynthesis while maintaining normal strain growth and development.

3.2. Identification of acetyl-CoA competition pathways in S. spinosa-pSET-cas9/sg-pyc

Considering that the biomass of *pyc* downregulated strain did not decrease, the observed increase in spinosad production was below expectations. Therefore, the underlying reasons for this limited increase were investigated. Quantitative analyses of pyruvate and acetyl-CoA were conducted in *S. spinosa*-pSET-*dcas9/sg-pyc*. The results showed significant pyruvate accumulation in *S. spinosa*-pSET-*dcas9/sg-pyc* (Fig. 3A), while acetyl-CoA contents remained largely unchanged on days 2 and 4, showing only a slight increase on day 8 (Fig. 3B). This is likely due to competition from pyruvate downstream metabolic pathways for acyl-CoA precursors.

Based on previous transcriptomic analyses, RT-qPCR was used to verify the expression of key genes in the downstream pyruvate metabolic pathway. The results showed that four key genes involved in the acetyl-CoA competitive metabolic pathways (TCA cycle and EMC pathway) in *S. spinosa*-pSET-*dcas9/sg-pyc* exhibited high transcription levels during the analyzed period (Figure S4, Fig. 3C). Therefore, these two pathways were chosen for downregulation to test the hypothesis.

3.3. CRISPRi-mediated inhibitory circuit downregulates key nodes in TCA cycle

Malonyl-CoA and methyl-malonyl-CoA, the two direct precursors of spinosad biosynthesis, are primarily derived from acetyl-CoA. The TCA cycle, the terminal metabolic pathway for sugars, lipids, and amino acids, plays a crucial role in sustaining cell growth and development by utilizing acetyl-CoA. Acetyl-CoA is consumed in the first step of the TCA cycle, where citrate synthase (EC 2.3.3.1) catalyzes its reaction with oxaloacetate to produce citrate. To redirect acetyl-CoA toward malonyl-CoA and methyl-malonyl-CoA biosynthesis and enhance spinosad yield, we attempted to downregulate the TCA cycle by suppressing *gltA* (citrate synthase encoding gene) expression.

Two *gltA* genes (orf 06851-4114, orf 06867-4125) were identified in the *S. spinosa* CCTCC M206084 genome and designated as *gltA1* and *gltA2*, respectively. The sgRNAs of *gltA1* and *gltA2* were designed to target nt 240–259 and nt 34–53 with respect to the start codon, respectively. The plasmids pSET-*dcas9/sg-gltA1* and pSET-*dcas9/sg-gltA2* were constructed and introduced into *S. spinosa*. The results indicated that spinosad production in *S. spinosa*-pSET-*dcas9/sg-gltA1* increased by 47.4 % (468 ± 29.5 mg/L), with a slight reduction in biomass, whereas spinosad production, biomass, and strain activity were significantly reduced in *S. spinosa*-pSET-*dcas9/sg-gltA2* (Fig. 4A and B). Transcription levels of *gltA1* and *gltA2* were measured in *S. spinosa*-pSET-*dcas9/sg-gltA1* and *S. spinosa*-pSET-*dcas9/sg-gltA2*, respectively. Compared with *S. spinosa*-pSET-*dcas9/sg-gltA1*, the transcription level of *S. spinosa*-pSET-*dcas9/sg-gltA2* was severely inhibited in all selected periods (Fig. 4C), which may account for the observed decline in spinosad titer, biomass, and strain activity in *S. spinosa*-pSET-*dcas9/sg-gltA2*.

The detection of precursors also indicated that the contents of three short-chain acyl-CoA (acetyl-CoA, malonyl-CoA and methyl-malonyl-CoA) in *S. spinosa*-pSET-*dcas9/sg-gltA1* were increased in different degrees (Fig. 4D, E, F). However, only elevated levels of acetyl-CoA and methyl-malonyl-CoA were observed in *S. spinosa*-pSET-*dcas9/sg-gltA2*, indicating that although inhibition of *gltA2* promoted the accumulation of acetyl-CoA to some degree, the conversion of acetyl-CoA to malonyl-CoA was also inhibited, which may be caused by the growth retardation of *S. spinosa*-pSET-*dcas9/sg-gltA2*.

3.4. CRISPRi-mediated inhibitory circuit downregulates key nodes in EMC pathway

The EMC pathway plays a critical role in modulating the flux of acetyl-CoA to adjust metabolic balance under different carbon sources or metabolic stress conditions. The first step of the EMC pathway involves

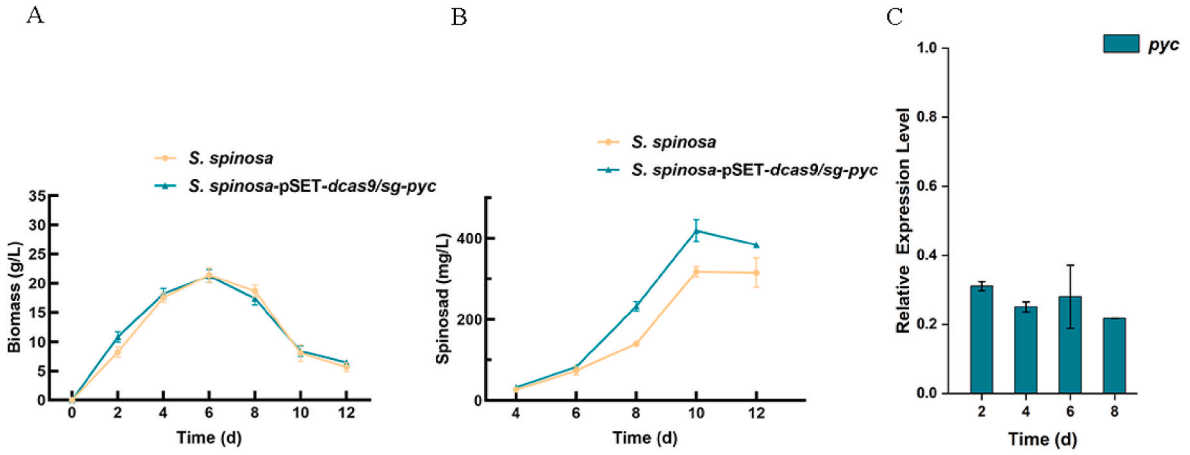

Fig. 2. Effects of CRISPRi-mediated downregulation of *pyc* in *S. spinosa*. **(A)** Biomass accumulation curve of *S. spinosa* and *S. spinosa*-pSET-*dcas9/sg-pyc*. **(B)** Spinosad accumulation of *S. spinosa* and *S. spinosa*-pSET-*dcas9/sg-pyc*. **(C)** Relative expression level of *pyc* gene in *S. spinosa*-pSET-*dcas9/sg-pyc* at 2nd, 4th, 6th, 8th day. Error bars are calculated from three independent determinations in each sample.

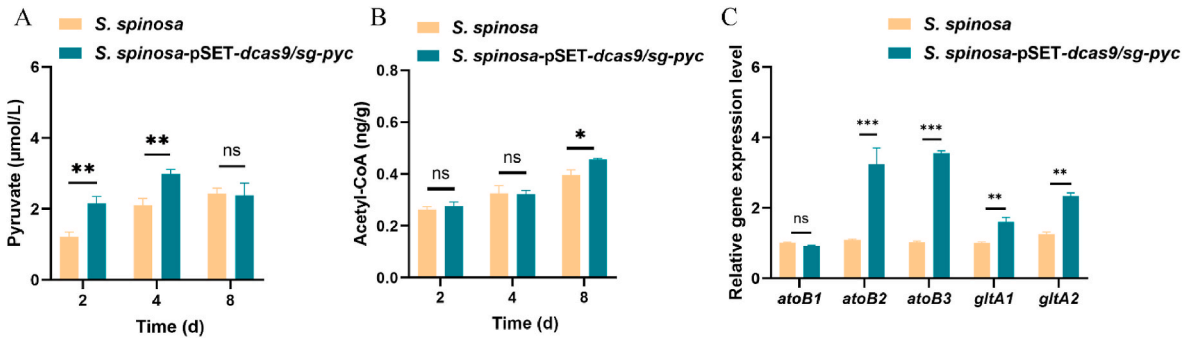

Fig. 3. Effects of *pyc* downregulation on precursors accumulation and key genes transcriptional levels involved in TCA cycle and ECM pathway. **(A)** Pyruvate accumulation of *S. spinosa* and *S. spinosa*-pSET-*dcas9/sg-pyc*. **(B)** Acetyl-CoA accumulation of *S. spinosa* and *S. spinosa*-pSET-*dcas9/sg-pyc*. **(C)** Transcriptional level of key genes involved in TCA cycle and ECM pathway of *S. spinosa* and *S. spinosa*-pSET-*dcas9/sg-pyc*. Error bars are calculated from three independent determinations in each sample. Univariate variance, $^{ns}P > 0.05$, $^{*}P < 0.05$, $^{**}P < 0.005$, $^{***}P < 0.001$.

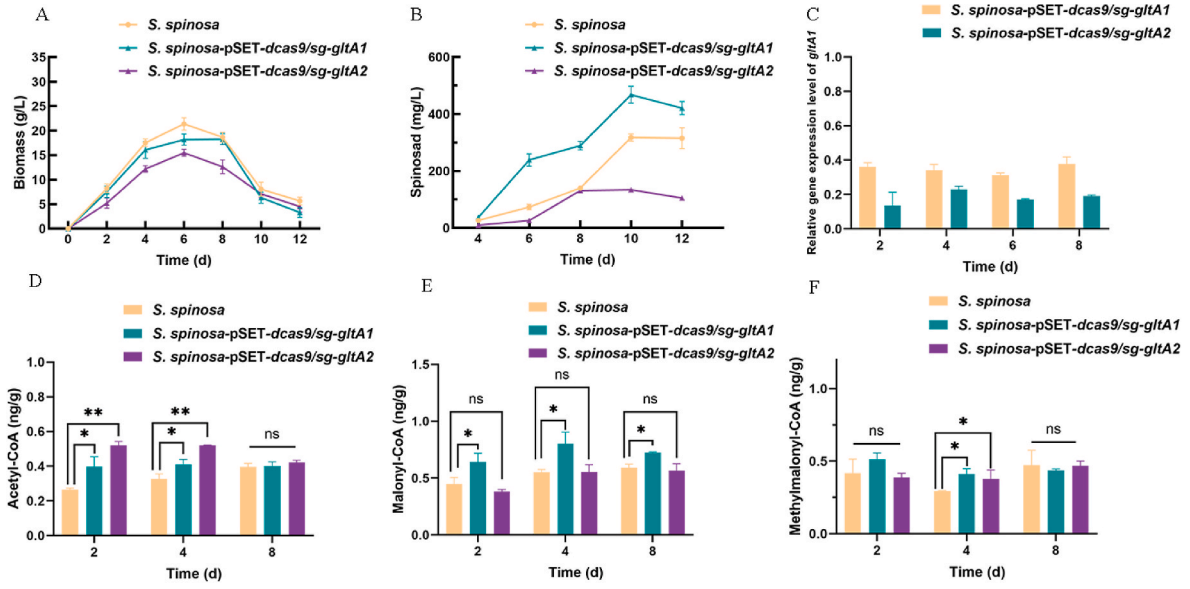

Fig. 4. Effects of CRISPRi-mediated downregulation of key nodes in TCA cycl. **(A)** Biomass accumulation curve of *S. spinosa*, *S. spinosa*-pSET-*dcas9/sg-gltA1* and *S. spinosa*-pSET-*dcas9/sg-gltA2*. **(B)** Spinosad accumulation curve of *S. spinosa*, *S. spinosa*-pSET-*dcas9/sg-gltA1* and *S. spinosa*-pSET-*dcas9/sg-gltA2*. **(C)** Relative expression level of *gltA1* and *gltA2* genes in *S. spinosa*-pSET-*dcas9/sg-gltA1* and *S. spinosa*-pSET-*dcas9/sg-gltA2*, respectively. **(D)** Concentrations of acetyl-CoA in *S. spinosa*, *S. spinosa*-pSET-*dcas9/sg-gltA1* and *S. spinosa*-pSET-*dcas9/sg-gltA2*. **(E)** Concentrations of malonyl-CoA in *S. spinosa*, *S. spinosa*-pSET-*dcas9/sg-gltA1* and *S. spinosa*-pSET-*dcas9/sg-gltA2*. **(F)** Concentrations of methyl-malonyl-CoA in *S. spinosa*, *S. spinosa*-pSET-*dcas9/sg-gltA1* and *S. spinosa*-pSET-*dcas9/sg-gltA2*. Error bars are calculated from three independent determinations in each sample. Univariate variance, $^{ns}P > 0.05$, $^{*}P < 0.05$, $^{**}P < 0.005$, $^{***}P < 0.001$.

the assimilation of acetyl-CoA, where acetyl-CoA is catalyzed by acetyl-CoA C-acetyltransferase (EC 2.3.1.9) to form acetoacetyl-CoA (https://www.kegg.jp/). As mentioned earlier, acetyl-CoA serves as a critical precursor for spinosad biosynthesis. Therefore, the acetyl-CoA C-acetyltransferase encoding genes were targeted for downregulation to attenuate the EMC pathway and mitigate acetyl-CoA competition.

The *S. spinosa* CCTCC M206084 genome contains 12 genes predicted to encode acetyl-CoA C-acetyltransferase. Based on previous transcriptomic analysis and RT-qPCR results (Figure S4, Fig. 3C), two *atoB* genes (orf 07451-4479 and orf 14507-8842) with high transcription levels were selected and renamed *atoB2* and *atoB3*, respectively. sgRNAs of *atoB2* and *atoB3* were designed to target nt 90–109 and nt 106–125 with respect to the start codon, respectively. Two plasmids (pSET-*dcas9/sg-atoB2* and pSET-*dcas9/sg-atoB3*) were constructed and introduced into *S. spinosa*. Analysis of spinosad titer revealed that respective repression of *atoB2* and *atoB3* resulted in an increased spinosad titer with a slight decline in biomass (Fig. 5A and B). Among these, *S. spinosa*-pSET-*dcas9/sg-atoB3* achieved a higher spinosad yield of 551.2 ± 27.2 mg/L, representing a 73.6 % increase compared to the original strain. RT-qPCR analysis showed that the relative transcriptional levels of *atoB2* and *atoB3* in *S. spinosa*-pSET-*dcas9/sg-atoB2* and *S. spinosa*-pSET-*dcas9/sg-atoB3* were reduced to 0.25–0.29 and 0.27–0.41, respectively (Fig. 5C).

The short-chain acyl-CoA content in *S. spinosa*-pSET-*dcas9/sg-atoB2* and *S. spinosa*-pSET-*dcas9/sg-atoB3* was measured, revealing that acetyl-CoA, malonyl-CoA, and methyl-malonyl-CoA all accumulated to varying degrees, with higher levels observed in *S. spinosa*-pSET-*dcas9/sg-atoB3* compared to *S. spinosa*-pSET-*dcas9/sg-atoB2* (Fig. 5D, E, F). These results demonstrated that the short-chain acyl-CoA content exhibited a positive correlation with spinosad yield within a specific range.

3.5. Combinatorial optimization of metabolic pathways to further increase spinosad production

As mentioned above, the downregulation of key nodes in the three core carbon metabolism pathways promoted the biosynthesis of spinosad individually, with *gltA1* and *atoB3* inhibition exhibiting greater effects compared to other genes in their respective pathways. Therefore,

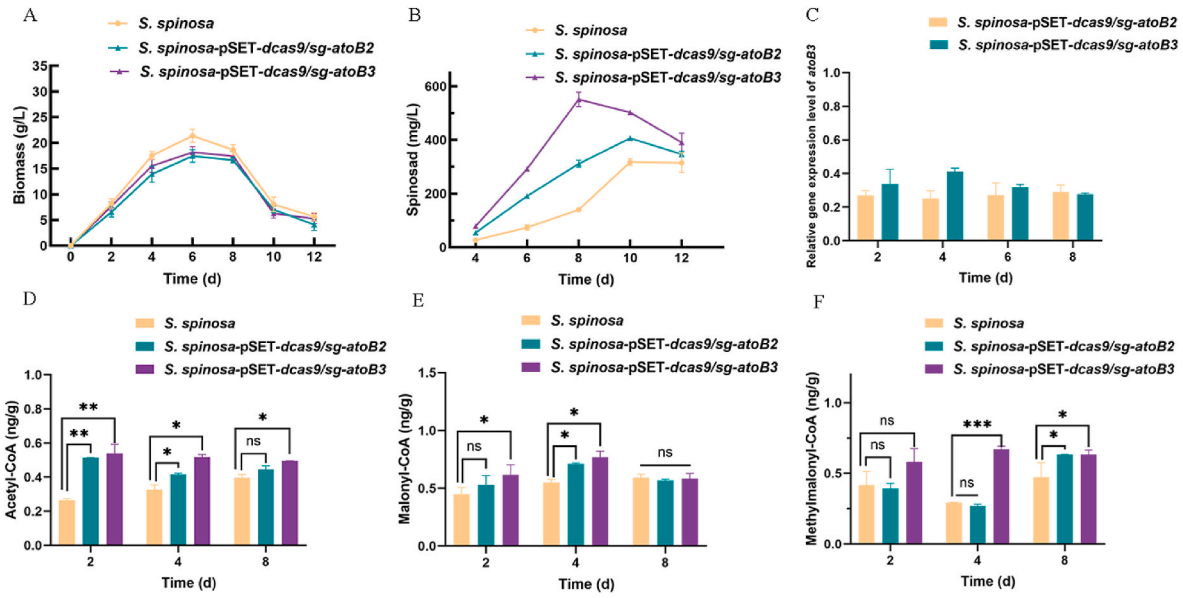

Fig. 5. Effects of CRISPRi-mediated downregulation of key nodes in EMC pathway. **(A)** Biomass accumulation curve of *S. spinosa*, *S. spinosa*-pSET-*dcas9/sg-atoB2* and *S. spinosa*-pSET-*dcas9/sg-atoB3*. **(B)** Spinosad accumulation curve of *S. spinosa*, *S. spinosa*-pSET-*dcas9/sg-atoB2* and *S. spinosa*-pSET-*dcas9/sg-atoB3*. **(C)** Relative expression level of *atoB2* and *atoB3* genes in *S. spinosa*, *S. spinosa*-pSET-*dcas9/sg-atoB2* and *S. spinosa*-pSET-*dcas9/sg-atoB3*, respectively. **(D)** Concentrations of acetyl-CoA in *S. spinosa*, *S. spinosa*-pSET-*dcas9/sg-atoB2* and *S. spinosa*-pSET-*dcas9/sg-atoB3*. **(E)** Concentrations of malonyl-CoA in *S. spinosa*, *S. spinosa*-pSET-*dcas9/sg-atoB2* and *S. spinosa*-pSET-*dcas9/sg-atoB3*. **(F)** Concentrations of methyl-malonyl-CoA in *S. spinosa*, *S. spinosa*-pSET-*dcas9/sg-atoB2* and *S. spinosa*-pSET-*dcas9/sg-atoB3*. Error bars are calculated from three independent determinations in each sample. Univariate variance, $^{ns}P > 0.05$, $^{*}P < 0.05$, $^{**}P < 0.005$, $^{***}P < 0.001$.

the three sgRNAs cassettes (promotor-*sg-pyc*-terminator, promotor-*sg-gltA1*-terminator, and promotor-*sg-atoB3*-terminator) were combined to construct a multigene CRISPRi downregulation circuit, and the plasmid pSET-*dcas9/sg-pyc/sg-gltA1/sg-atoB3* was introduced into *S. spinosa* and verified (Fig. S5A). However, the *pyc-gltA1-atoB3* downregulated strain PCA1B3 exhibited marked growth retardation and significantly reduced spinosad production (Fig. 6A and B). This suggests that simultaneous downregulation of these three target genes at the current inhibition level may cause metabolism imbalance, resulting in an insufficient supply of metabolites for primary metabolism, and, consequently, growth retardation and reduced spinosad titer.

It is reported that the farther the sgRNA is positioned from the start codon of the target gene, the weaker the inhibitory effect of CRISPRi [13,27]. Therefore, we adjusted the downregulation strength by altering the position of sgRNA on the target gene. Since there was no biomass decrease in *pyc* downregulated strain, optimizations of sgRNA were conducted in *gltA1* and *atoB3*. sgRNAs positioned farther from the start codon of *gltA1* and *atoB3* were redesigned to target nt 492–511 (*sg-gltA11*) and nt 416–435 (*sg-atoB31*) with respect to the start codon, respectively. Subsequently, three permutations of *sg-gltA1*, *sg-gltA11*, *sg-atoB3*, and *sg-atoB31* were connected with *sg-pyc* (all sequences contain a promoter and a terminator, respectively), and the corresponding multigene downregulation plasmids were transferred into *S. spinosa* (Fig. 6C).

The results indicated that after sgRNA optimization, both biomass and spinosad production significantly increased compared to PCA1B3, with PCA11B (the strain carrying pSET-*dcas9/sg-pyc/sg-gltA11/sg-atoB3*) showing the highest spinosad titer, reaching 633.1 ± 38.6 mg/L (Fig. 6D and E). It was confirmed that the CRISPRi repression strength can be adjusted by modifying the sgRNAs targeting position. It is worth mentioning that the target location of *sg-gltA11* and *sg-atoB31* were farer away from the start codon than *sg-gltA1* and *sg-atoB3*. As a result, the inhibition of *gltA1* and *atoB3* in multigene downregulation strains was weakened while the relative expression fold of *pyc* showed no significant change (Figs. S5B, C, D). The results of pyruvate and shore-chain acyl-CoA determination also consistent with the previous results in single-gene repression strains (Fig. S6). Additionally, PCA11B3 was confirmed to exhibit stable spinosad production after five subcultures (Fig. S7).

3.6. Proteomic and transcriptional level analysis of spinosad biosynthesis in PCA11B3

The spinosad gene cluster mainly contains 23 genes, of which 19 *spn* genes (*spnA–S*) are related to forosamine biosynthesis, polyketide brid-ing, tri-*O*-methylrhamnose biosynthesis and polyketide biosynthesis. The expression level of *spn* genes is directly related to the biosynthesis of spinosad. Therefore, 12 *spn* genes were selected according to different transcription directions for RT-qPCR to evaluate their expression levels (Fig. 7A). As we expected, most of the selected *spn* genes in PCA11B3 were upregulated, which directly caused the increase in spinosad titer.

To further analyze how spinosad biosynthesis is promoted in PCA11B3, non-labeled data-independent acquisition (DIA) quantitative proteome technology was conducted to evaluate the protein expression level and corresponding biological function in PCA11B3. Differential expression proteins (DEPs) were identified by screening for fold change (FC) greater than 5 times or less than 0.2 times. A total of 784 DEPs were founded in PCA11B3, of which 661 were upregulated and 123 down-regulated. Enrichment analysis of KEGG secondary classification suggesting that the DEPs mainly involved in pathways of glycolysis/gluconeogenesis (20), pyruvate metabolism (19), ribosome (16), citrate cycle (14), glyoxylate and dicarboxylate metabolism (13), and Biosynthesis of amino acids (32), etc (Fig. 7B). The above results indicated that multigene repression of *pyc*, *gltA1*, and *atoB3* affected the overall metabolic network of *S. spinosa*. A major metabolic network map was constructed based on the data identified in the comparative proteomic data to illustrate the promotion of spinosad biosynthesis in PCA11B3, including the main pathways involved in pyruvate and acetyl-coA metabolism, such as glycolysis/gluconeogenesis, TCA cycle, glyoxylate metabolism, and amino acid metabolism. (Fig. 7C). The inhibition of *pyc* reduced the metabolic flux of pyruvate in gluconeogenesis, which is then converted to acetyl-CoA. The repression of *gltA1* and *atoB3* not only weaken the TCA cycle but also reduce glyoxylate production. In addition, the metabolic pathways of multiple amino acids are enhanced,

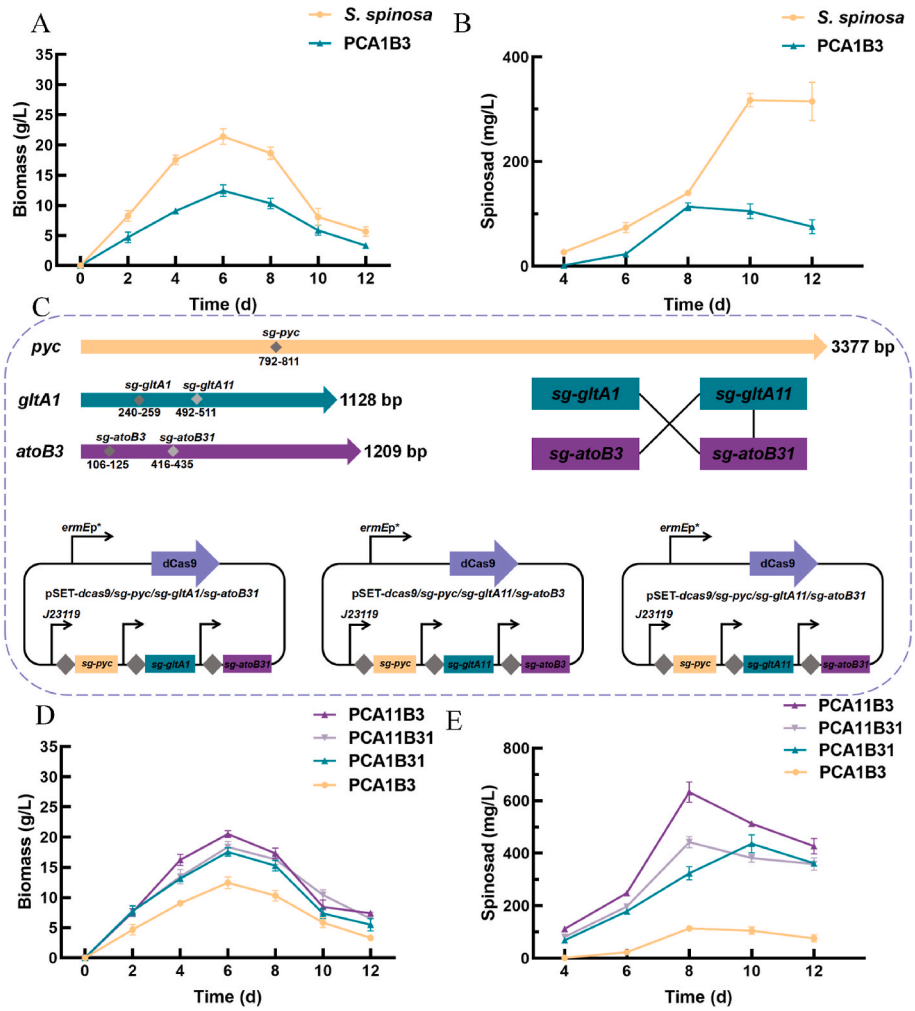

Fig. 6. Optimization of sgRNA and effects of CRISPRi-mediated multigene downregulation. **(A, D)** Biomass accumulation curve of *S. spinosa*, PCA1B3, PCA11B3, PCA1B31 and PCA11B31. **(B, E)** Spinosad accumulation of *S. spinosa*, PCA1B3, PCA11B3, PCA1B31 and PCA11B31. **(C)** Schematic design of sgRNAs. Error bars are calculated from three independent determinations in each sample.

thereby providing a large number of precursors for the spinosad biosynthesis. These results demonstrated the feasibility of CRISPRi-based static multigene regulation in spinosad synthesis networks.

4. Discussion

In this study, we employed the CRISPRi technology to regulate the core carbon metabolic pathways in *S. spinosa*, exploring the possibility of optimizing spinosad biosynthesis through multigene downregulation. By simultaneously downregulating the *pyc*, *gltA1*, and *atoB3* genes, we successfully altered the metabolic flux and significantly increased spinosad production. This study highlights the potential of CRISPRi technology in metabolic engineering and provides valuable insights for future metabolic optimization strategies.

We firstly repressed *pyc* gene and resulted an increase in the concentration of pyruvate and spinosad. This result suggests that the downregulation of *pyc* caused a significant shift in the metabolic flux of pyruvate, reducing the carbon flow through gluconeogenesis and directing more carbon resources towards spinosad biosynthesis. This finding supports our hypothesis that reducing the overutilization of pyruvate can enhance the production of spinosad. Previous studies have also reported that pyruvate accumulation is commonly observed in high-yield spinosyn-producing engineered strains [28,37], which aligns with the phenomena observed in our experiment. Yang et al. When we downregulated *gltA1* and *atoB3* genes, a significant accumulation of acetyl-CoA, malonyl-CoA, and methylmalonyl-CoA were observed. These short-chain acyl-CoA are key precursors in spinosad biosynthesis, and increasing their accumulation within the cell can directly promote spinosad production [38,39], indicating that inhibition of the TCA cycle and the EMC pathway facilitated the more efficient utilization of short-chain acyl-CoA for spinosad synthesis.

However, when *pyc*, *gltA1*, and *atoB3* were repressed simultaneously, the strain occurred growth retardation and metabolic imbalance, suggesting that excessive inhibition of these metabolic pathways led to a shortage of essential metabolites, disrupting normal cell growth and metabolism. By further optimizing the CRISPRi system and adjusting the targeting positions of the sgRNAs, we found that reducing the repression strength of *gltA1* and *atoB3* helped avoid metabolic imbalance and further promoted spinosad synthesis. Ultimately, the PCA11B3 strain exhibited the highest spinosad titer.

Interestingly, the simultaneous regulation of *pyc*, *gltA1*, and *atoB3* (in PCA11B3) led to changes in the transcription levels of many *spn* genes. The metabolic pathways in which these genes are located directly affect the supply of carbon sources and energy within the cell, thereby indirectly regulating the precursor and metabolic environment required for spinosad synthesis (the target product of *spn* genes). In PCA11B3, the concentration of key intracellular metabolites such as acetyl-CoA is significantly increased, and the accumulation of acetyl-CoA can upregulate the synthesis of secondary metabolites by activating transcription factors or specific regulatory mechanisms [40,41]. In addition,

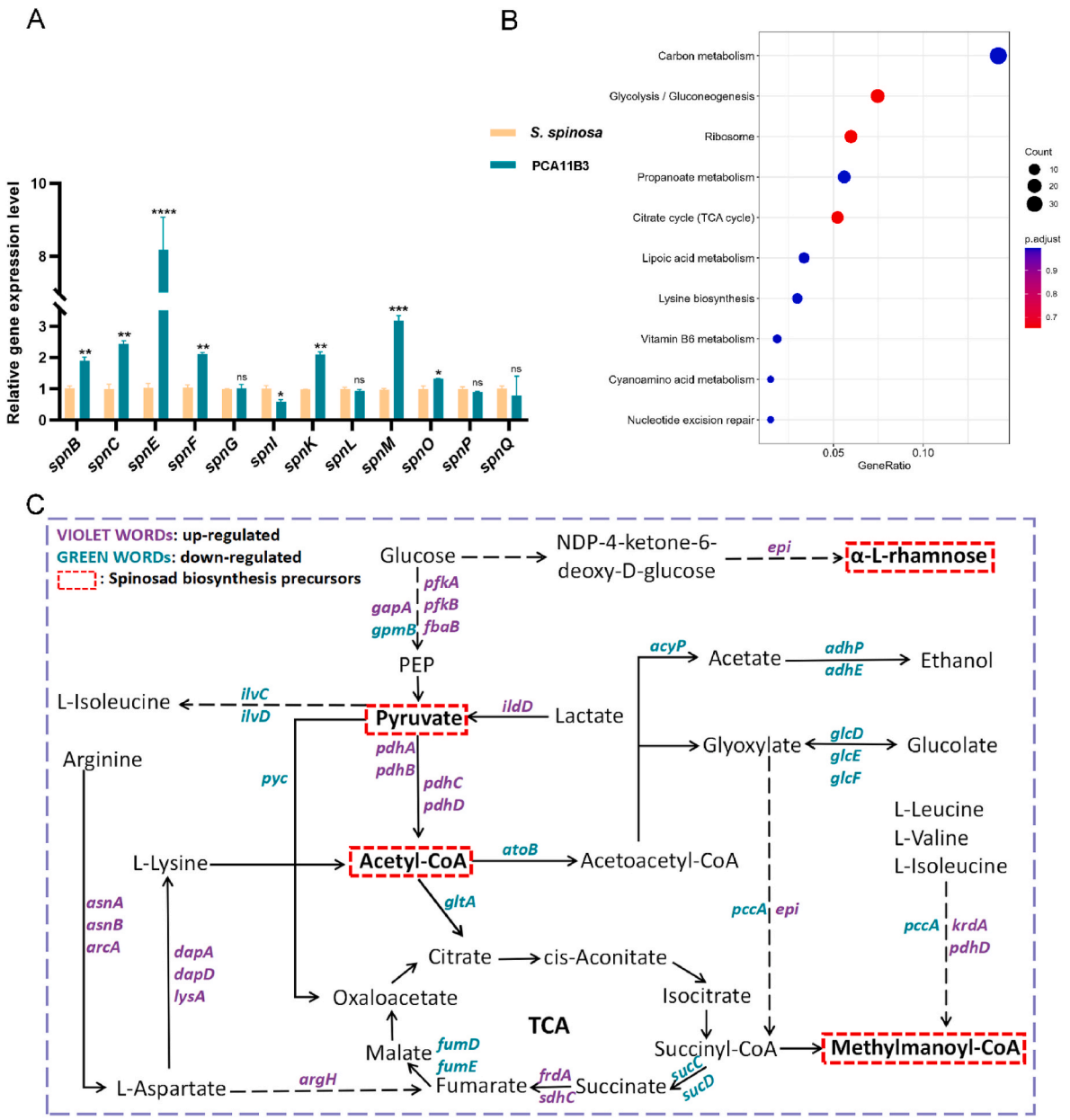

Fig. 7. Effects of multigene downregulation on Spn family genes and metabolism of PCA11B3. **(A)** Relative expression level of representative *spn* genes in strain PCA11B3. **(B)** Bubble plot of the most significant pathways with KEGG enrichment of DEPs. **(C)** Mainly metabolic pathways with DEPs related with spinosad biosynthesis in PCA11B3. Error bars are calculated from three independent determinations in each sample.

the downregulation of *pyc*, *gltA1* and *atoB3* not only directly affects the accumulation of short-chain acyl-CoA, but also indirectly affects the transcription of *spn* genes by regulating the TCA cycle, glycolysis, amino acid metabolism and other pathways (Fig. 7).

The results of this study demonstrate that downregulation of *pyc*, *gltA1*, and *atoB3* can effectively reconfigure the metabolic flux within the cell, optimizing spinosad biosynthesis. Specifically, downregulation of *pyc* reduced the carbon flux through gluconeogenesis and lowered the consumption of pyruvate, allowing more carbon to flow into the spinosad biosynthetic pathway. Simultaneously, the downregulation of *gltA1* and *atoB3* slowed the activity of the TCA cycle and the EMC pathway, leading to the accumulation of acetyl-CoA and providing more precursors for spinosad synthesis. The accumulation of acetyl-CoA not only promoted spinosad biosynthesis but also enhanced the levels of other short-chain acyl-CoA intermediates (e.g., malonyl-CoA and methylmalonyl-CoA), further boosting spinosad production. However, excessive inhibition of these key metabolic pathways could lead to metabolic imbalance, resulting in growth suppression and a decline in production. Thus, balancing the repression strength of these pathways and avoiding excessive suppression are crucial for optimizing spinosad yield.

At present, there have been a lot of studies focused on the positive related enzymes in the spinosad synthesis pathway, but few studies on the metabolic flow competition in the precursor branched-chain metabolic pathway or essential metabolic pathway [30,39–42]. This study utilizes a CRISPRi multigene downregulation strategy, achieving significant progress in enhancing spinosad biosynthesis. Compared to previous studies focusing on single-gene regulation or specific pathway modifications, our approach demonstrated stronger potential for metabolic engineering. Prior research has utilized genetic engineering to regulate spinosad biosynthetic pathways, but most studies have concentrated on single gene regulation or targeting specific pathways

[43–45]. In contrast, by simultaneously downregulating multiple key nodes using CRISPRi technology, we successfully enhanced spinosad production and optimized metabolic flux. This strategy offers a novel approach for metabolic engineering. Although we made significant strides in optimizing the spinosad biosynthetic pathway, growth retardation and metabolic imbalance remain notable challenges when metabolic pathways are excessively downregulated. Future research can focus on fine-tuning CRISPRi repression strength to avoid metabolic flux imbalance while further improving the yield.

In conclusion, this study successfully optimized the metabolic pathways in *S. spinosa* through multigene downregulation using CRISPRi technology, significantly increasing spinosad production and providing new insights into metabolic engineering. Our findings demonstrate that fine-tuning metabolic flux, especially through multigene downregulation strategies, can effectively enhance the synthesis of target products. While challenges related to metabolic imbalance remain, with further optimization of the CRISPRi system, this approach holds great promise for the production of other natural products in the future.

CRediT authorship contribution statement

Zirong Zhu: Writing – original draft, Methodology, Conceptualization. **Li Cao:** Writing – review & editing. **Ziyuan Xia:** Visualization, Software, Investigation. **Xirong Liu:** Visualization, Software, Investigation. **Wangqion Chen:** Visualization, Software, Investigation. **Zirui Dai:** Writing – review & editing. **Duo Jin:** Writing – review & editing. **Jie Rang:** Funding acquisition. **Shengbiao Hu:** Supervision. **Liqiu Xia:** Supervision, Methodology, Funding acquisition.

Funding information

This work was supported by funding from the National Natural Science Foundation of China (31770106, 32200062) and the Natural Science Foundation of Hunan Province (2024JJ5258).

Declaration of competing interest

The authors declare the following financial interests/personal relationships which may be considered as potential competing interests: XirongLiu is currently employed by Hunan Norchem Pharmaceutical Co., Ltd.

Appendix A. Supplementary data

Supplementary data to this article can be found online at https://doi.org/10.1016/j.synbio.2025.02.010.

References

[1] Scott M, Gunderson CW, Mateescu EM, Zhang Z, Hwa T. Interdependence of cell growth and gene expression: origins and consequences. Science 2010;330(6007):1099–102. https://doi.org/10.1126/science.1192588.

[2] Na D, Kim TY, Lee SY. Construction and optimization of synthetic pathways in metabolic engineering. Curr Opin Microbiol 2010;13(3):363–70. https://doi.org/10.1016/j.mib.2010.02.004.

[3] Koffas MAG, Jung GY, Stephanopoulos G. Engineering metabolism and product formation in *Corynebacterium glutamicum* by coordinated gene overexpression. Metab Eng 2003;5(1):32–41. https://doi.org/10.1016/s1096-7176(03)00002-8.

[4] Kim ES. Recent advances of actinomycetes. Biomolecules 2021;11(2):134. https://doi.org/10.3390/biom11020134.

[5] Ngamcharungchit C, Chaimusik N, Panbangred W, Euanorasetr J, Intra B. Bioactive metabolites from terrestrial and marine actinomycetes. Molecules 2023;28(15):5915. https://doi.org/10.3390/molecules28155915.

[6] Biggs BW, De Paepe B, Santos CN, De Mey M, Kumaran Ajikumar P. Multivariate modular metabolic engineering for pathway and strain optimization. Curr Opin Biotechnol 2014;29:156–62. https://doi.org/10.1016/j.copbio.2014.05.005.

[7] Palazzotto E, Tong Y, Lee SY, Weber T. Synthetic biology and metabolic engineering of actinomycetes for natural product discovery. Biotechnol Adv 2019;37(6):107366. https://doi.org/10.1016/j.biotechadv.2019.03.005.

[8] Stegmüller J, Rodríguez Estévez M, Shu W, Gläser L, Myronovskyi M, Rückert-Reed C, Kalinowski J, Luzhetskyy A, Wittmann C. Systems metabolic engineering of the primary and secondary metabolism of *Streptomyces albidoflavus* enhances production of the reverse antibiotic nybomycin against multi-resistant *Staphylococcus aureus*. Metab Eng 2024;81:123–43. https://doi.org/10.1016/j.ymben.2023.12.004.

[9] Wang L, Yang H, Wu M, Zhang H, Zhang J, Chen X. Enhanced ε-poly-L-lysine production in *Streptomyces albulus* through multi-omics-guided metabolic engineering. Biomolecules 2024;14(7):752. https://doi.org/10.3390/biom14070752.

[10] Zhuang Z, Kong W, Wen Z, Tong N, Lin J, Zhang F, Fan Z, Yi L, Huang Y, Duan Y, Yan X, Zhu X. Combinatorial metabolic engineering of *Streptomyces* sp. CB03234-S for the enhanced production of anthraquinone-fused enediyne tiancimycins. Microb Cell Fact 2024;23(1):128. https://doi.org/10.1186/s12934-024-02399-w.

[11] Yu W, Jin K, Wu Y, Zhang Q, Liu Y, Li J, Du G, Chen J, Lv X, Ledesma-Amaro R, Liu L. A pathway independent multi-modular ordered control system based on thermosensors and CRISPRi improves bioproduction in *Bacillus subtilis*. Nucleic Acids Res 2022;50(11):6587–600. https://doi.org/10.1093/nar/gkac476.

[12] Holtz WJ, Keasling JD. Engineering static and dynamic control of synthetic pathways. Cell Biochem Funct 2010;140(1):19–23. https://doi.org/10.1016/j.cell.2009.12.029.

[13] Tian J, Yang G, Gu Y, Sun X, Lu Y, Jiang W. Developing an endogenous quorum-sensing based CRISPRi circuit for autonomous and tunable dynamic regulation of multiple targets in *Streptomyces*. Nucleic Acids Res 2020;48(14):8188–202. https://doi.org/10.1093/nar/gkaa602.

[14] Cress BF, Trantas EA, Ververidis F, Linhardt RJ, Koffas MA. Sensitive cells: enabling tools for static and dynamic control of microbial metabolic pathways. Curr Opin Biotechnol 2015;36:205–14. https://doi.org/10.1016/j.copbio.2015.09.007.

[15] Li L, Zhao Y, Ruan L, Yang S, Ge M, Jiang W, Lu Y. A stepwise increase in pristinamycin II biosynthesis by *Streptomyces pristinaespiralis* through combinatorial metabolic engineering. Metab Eng 2015;29:12–25. https://doi.org/10.1016/j.ymben.2015.02.001.

[16] Zhao D, Zhu X, Zhou H, Sun N, Wang T, Bi C, Zhang X. CRISPR-based metabolic pathway engineering. Metab Eng 2021;63:148–59. https://doi.org/10.1016/j.ymben.2020.10.004.

[17] Gupta A, Reizman IM, Reisch CR, Prather KL. Dynamic regulation of metabolic flux in engineered bacteria using a pathway-independent quorum-sensing circuit. Nat Biotechnol 2017;35(3):273–9. https://doi.org/10.1038/nbt.3796.

[18] Tian T, Kang JW, Kang A, Lee TS. Redirecting metabolic flux via combinatorial multiplex CRISPRi-mediated repression for isopentenol production in *Escherichia coli*. ACS Synth Biol 2019;8(2):391–402. https://doi.org/10.1021/acssynbio.8b00429.

[19] Al-Fadhli AA, Threadgill MD, Mohammed F, Sibley P, Al-Ariqi W, Parveen I. Macrolides from rare actinomycetes: structures and bioactivities. Int J Antimicrob Agents 2022;59(2). https://doi.org/10.1016/j.ijantimicag.2022.106523.

[20] Ding T, Yang L-J, Zhang W-D, Shen Y-H. The secondary metabolites of rare actinomycetes: chemistry and bioactivity. RSC Adv 2019;9(38):21964–88. https://doi.org/10.1039/c9ra03579f.

[21] Guojun Y, Yuping H, Yan J, Kaichun L, Haiyang X. A new medium for improving spinosad production by *Saccharopolyspora spinosa*. Jundishapur J Microbiol 2016;9(6):e16765. https://doi.org/10.5812/jjm.16765.

[22] Sarfraz M, Dosdall LM, Keddie BA. Spinosad: a promising tool for integrated pest management. Outlooks Pest Manag 2005;16(2):78–84. https://doi.org/10.1564/16apl09.

[23] Huang K-x, Xia L, Zhang Y, Ding X, Zahn JA. Recent advances in the biochemistry of spinosyns. Appl Microbiol Biotechnol 2009;82:13–23. https://doi.org/10.1007/s00253-008-1784-8.

[24] Xue C, Zhang X, Yu Z, Zhao F, Wang M, Lu W. Up-regulated spinosad pathway coupling with the increased concentration of acetyl-CoA and malonyl-CoA contributed to the increase of spinosad in the presence of exogenous fatty acid. Biochem Eng J 2013;81:47–53. https://doi.org/10.1016/j.bej.2013.10.004.

[25] Zhao M, Wang M, Wang S, Xiong L, Gao B, Liu M, Tao X, Wang FQ, Wei D. A self-sustained system spanning the primary and secondary metabolism stages to boost the productivity of *Streptomyces*. ACS Synth Biol 2022;11(1):353–65. https://doi.org/10.1021/acssynbio.1c00473.

[26] Gilbert LA, Larson MH, Morsut L, Liu Z, Brar GA, Torres SE, Stern-Ginossar N, Brandman O, Whitehead EH, Doudna JA, Lim WA, Weissman JS, Qi LS. CRISPR-mediated modular RNA-guided regulation of transcription in eukaryotes. Cell 2013;154(2):442–51. https://doi.org/10.1016/j.cell.2013.06.044.

[27] Qi LS, Larson MH, Gilbert LA, Doudna JA, Weissman JS, Arkin AP, Lim WA. Repurposing CRISPR as an RNA-guided platform for sequence-specific control of gene expression. Cell 2013;152(5):1173–83. https://doi.org/10.1016/j.cell.2013.02.022.

[28] Liu Z, Zhu Z, Tang J, He H, Wan Q, Luo Y, Huang W, Yu Z, Hu Y, Ding X, Xia L. RNA-Seq-Based transcriptomic analysis of *Saccharopolyspora spinosa* revealed the critical function of PEP phosphonomutase in the replenishment pathway. J Agric Food Chem 2020;68(49):14660–9. https://doi.org/10.1021/acs.jafc.0c04443.

[29] Tang J, He H, Li Y, Liu Z, Xia Z, Cao L, Zhu Z, Shuai L, Liu Y, Wan Q, Luo Y, Zhang Y, Rang J, Xia L. Comparative proteomics reveals the effect of the transcriptional regulator Sp13016 on butenyl-spinosyn biosynthesis in *Saccharopolyspora pogona*. J Agric Food Chem 2021;69(42):12554–65. https://doi.org/10.1021/acs.jafc.1c03654.

[30] Cao L, Liu Y, Sun L, Zhu Z, Yang D, Xia Z, Jin D, Dai Z, Rang J, Xia L. Enhanced triacylglycerol metabolism contributes to the efficient biosynthesis of spinosad in *Saccharopolyspora spinosa*. Synth Syst Biotechnol 2024;9(4):809–19. https://doi.org/10.1016/j.synbio.2024.06.007.

[31] Zhao Y, Li L, Zheng G, Jiang W, Deng Z, Wang Z, Lu Y. CRISPR/dCas9-Mediated multiplex gene repression in *Streptomyces*. Biotechnol J 2018;13(9). https://doi.org/10.1002/biot.201800121.

[32] Tang J, Zhu Z, He H, Liu Z, Xia Z, Chen J, Hu J, Cao L, Rang J, Shuai L, Liu Y, Sun Y, Ding X, Hu S, Xia L. Bacterioferritin: a key iron storage modulator that affects strain growth and butenyl-spinosyn biosynthesis in *Saccharopolyspora pogona*. Microb Cell Fact 2021;20(1). https://doi.org/10.1186/s12934-021-01651-x.

[33] He H, Tang J, Chen J, Hu J, Zhu Z, Liu Y, Shuai L, Cao L, Liu Z, Xia Z, Ding X, Hu S, Zhang Y, Rang J, Xia L. Flaviolin-like gene cluster deletion optimized the butenyl-spinosyn biosynthesis route in *Saccharopolyspora pogona*. ACS Synth Biol 2021;10 (10):2740–52. https://doi.org/10.1021/acssynbio.1c00344.

[34] Gao C, Guo L, Hu G, Liu J, Chen X, Xia X, Liu L. Engineering a CRISPRi circuit for autonomous control of metabolic flux in *Escherichia coli*. ACS Synth Biol 2021;10 (10):2661–71. https://doi.org/10.1021/acssynbio.1c00294.

[35] Zhang Y, Liu X, Yin T, Li Q, Zou Q, Huang K, Guo D, Zhang X. Comparative transcriptomic analysis of two *Saccharopolyspora spinosa* strains reveals the relationships between primary metabolism and spinosad production. Sci Rep 2021; 11(1). https://doi.org/10.1038/s41598-021-94251-z.

[36] Yang Q, Ding X, Liu X, Liu S, Sun Y, Yu Z, Hu S, Rang J, He H, He L, Xia L. Differential proteomic profiling reveals regulatory proteins and novel links between primary metabolism and spinosad production in *Saccharopolyspora spinosa*. Microb Cell Fact 2014;13(1):27. https://doi.org/10.1186/1475-2859-13-27.

[37] Zhu Z, Chen W, Cao L, Xia Z, Rang J, Hu S, Xia L. ARTP/NTG compound mutagenesis improved the spinosad production and the insecticidal virulence of *Saccharopolyspora spinosa*. Int J Mol Sci 2024;25(22). https://doi.org/10.3390/ijms252212308.

[38] Li J, Mu X, Dong W, Chen Y, Kang Q, Zhao G, Hou J, Gonzalez R, Bai L, Feng Y, Yang C, Liu T, Tan Z. A non-carboxylative route for the efficient synthesis of central metabolite malonyl-CoA and its derived products. Nat Catal 2024;7(4):361–74. https://doi.org/10.1038/s41929-023-01103-2.

[39] Zhang Y, Liu X, Yin T, Li Q, Zou Q, Huang K, Guo D, Zhang X. Comparative transcriptomic analysis of two *Saccharopolyspora spinosa* strains reveals the relationships between primary metabolism and spinosad production. Sci Rep 2021; 11(1):14779. https://doi.org/10.1038/s41598-021-94251-z.

[40] Bridget AF, Nguyen CT, Magar RT, Sohng JK. Increasing production of spinosad in *Saccharopolyspora spinosa* by metabolic engineering. Biotechnol Appl Biochem 2022;70(3):1035–43. https://doi.org/10.1002/bab.2418.

[41] Liu Z, Xiao J, Tang J, Liu Y, Shuai L, Cao L, Xia Z, Ding X, Rang J, Xia L. Effects of *acuC* on the growth development and spinosad biosynthesis of *Saccharopolyspora spinosa*. Microb Cell Fact 2021;20(1):141. https://doi.org/10.1186/s12934-021-01630-2.

[42] Tao H, Zhang Y, Deng Z, Liu T. Strategies for enhancing the yield of the potent insecticide spinosad in actinomycetes. Biotechnol J 2018;14(1):e1700769. https://doi.org/10.1002/biot.201700769.

[43] Liu Z, Xiao J, Tang J, Liu Y, Shuai L, Cao L, Xia Z, Ding X, Rang J, Xia L. Effects of acuC on the growth development and spinosad biosynthesis of *Saccharopolyspora spinosa*. Microb Cell Fact 2021;20(1). https://doi.org/10.1186/s12934-021-01630-2.

[44] Cao L, Zhu Z, Qin H, Xia Z, Xie J, Li X, Rang J, Hu S, Sun Y, Xia L. Effects of a Pirin-like protein on strain growth and spinosad biosynthesis in *Saccharopolyspora spinosa*. Appl Microbiol Biotechnol 2023;107(17):5439–51. https://doi.org/10.1007/s00253-023-12636-8.

[45] Mu X, Lei R, Yan S, Deng Z, Liu R, Liu T. The LysR family transcriptional regulator ORF-L16 regulates spinosad biosynthesis in *Saccharopolyspora spinosa*. Synth Syst Biotechnol 2024;9(4):609–17. https://doi.org/10.1016/j.synbio.2024.05.001.